EUROPHYSICS LETTERS 15 May 2006

Europhys. Lett., **74** (4), pp. 665–671 (2006)
DOI: 10.1209/epl/i2006-10026-8

Evolution of interface patterns of three-dimensional two-layer liquid films

A. Pototsky[1], M. Bestehorn[1], D. Merkt[1] and U. Thiele[2]

[1] *Lehrstuhl für Theoretische Physik II, Brandenburgische Technische Universität Cottbus - Erich-Weinert-Straße 1, D-03046 Cottbus, Germany*
[2] *Max-Planck-Institut für Physik komplexer Systeme - Nöthnitzer Straße 38 D-01187 Dresden, Germany*

received 18 January 2006; accepted in final form 27 March 2006
published online 14 April 2006

PACS. 68.15.+e – Liquid thin films.
PACS. 81.16.Rf – Nanoscale pattern formation.
PACS. 68.55.-a – Thin film structure and morphology.

Abstract. – The structuring process of two-layer liquid films driven by van der Waals interactions is investigated numerically for three-dimensional systems. Different types of dynamical transitions of the interface morphologies are characterised using coupled evolution equations for the thickness profiles. We introduce a global deflection measure that faithfully captures the transitions occurring in the course of the short- and long-time evolution. Using an Si/PMMA/PS/air system as example, transitions via branch switching and via coarsening are analysed in detail.

The dewetting of ultrathin liquid films with thicknesses below 100 nm is normally caused by long-range van der Waals interactions between the molecules of the gas, the liquid(s) and the substrate [1, 2]. For a one-layer film of thickness h the corresponding excess interface energy per unit area is $\Phi(h) \sim 1/h^2$. Dewetting is initiated by a surface instability if the second derivative $\mathrm{d}^2\Phi/\mathrm{d}h^2$ is negative [3, 4]. Besides the resulting short-time film-rupture dynamics the dependence $\Phi(h)$ also dictates the long-time evolution, *i.e.* it determines the morphology of the surface patterns appearing at early times as well as morphology changes at later times. In the one-layer case three different morphologies are possible: drops, holes and as an intermediate, mazes or labyrinths [5]. If the linearly unstable film thickness range is bounded from below and above by finite metastable ranges, *i.e.* a Maxwell construction results in two finite equilibrium thicknesses ($h_{\min}$ and $h_{\max}$ in fig. 1a, cf. also [4, 6]), then drops (holes) form for an initial film thickness h_0 left (right) of the Maxwell point [5, 7]. For h_0 close to the Maxwell point mazes prevail in the short-time evolution.

However, the pattern morphology may change in the course of the time evolution depending on the existence of the upper boundary of metastability. If $h_{\max} < \infty$ exists (as for the disjoining pressure $-\mathrm{d}\Phi/\mathrm{d}h$ in fig. 1a), the morphology does not change [5, 7], *i.e.* drops coarsen to drops and holes coarsen to holes. On the contrary, if $h_{\max} < \infty$ does not exist (fig. 1b), the evolution may start with a hole pattern which during coarsening turns into a drop pattern [8].

© EDP Sciences
Article published by EDP Sciences and available at http://www.edpsciences.org/epl or http://dx.doi.org/10.1209/epl/i2006-10026-8

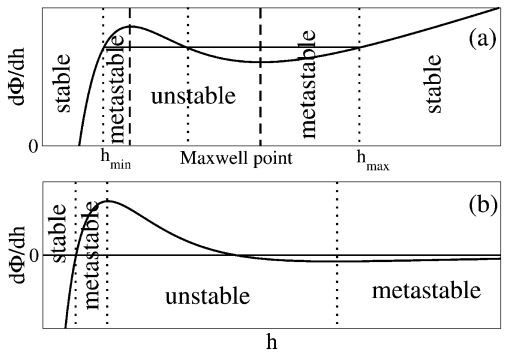

Fig. 1

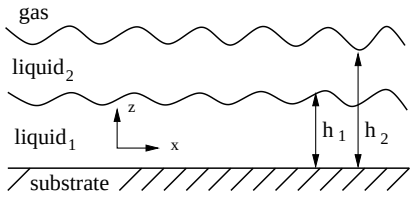

Fig. 2

Fig. 1 – Shown is the first derivative for two excess interface energies (corresponding to the negative disjoining pressure). (a) Combination of the Pismen-Pomeau pressure with a hydrostatic term $\mathrm{d}\Phi/\mathrm{d}h = 2\exp[-h][1-\exp[-h]] + 0.05h$ [9, 10]. (b) Combination of a stabilizing long-range van der Waals with a destabilizing short-range polar interaction $\mathrm{d}\Phi/\mathrm{d}h = -b/h^3 + \exp[-h]$ [10, 11], with $b = 1$. Vertical dotted lines indicate boundaries between unstable, stable and metastable film thickness ranges. They result either from the condition $\mathrm{d}^2\Phi/\mathrm{d}h^2 = 0$, or from the Maxwell construction. In (b) the stable-metastable boundary is obtained from $\mathrm{d}\Phi/\mathrm{d}h = 0$.

Fig. 2 – Sketch of the two-layer film. Note that h_1 and h_2 are the thickness of the lower layer and the overall thickness, respectively.

In this letter we investigate different types of morphological transitions that may occur in dewetting two-layer films. First experimental results show already intricate behaviour not known from one-layer films [12–15]. Here, we show that results obtained for two-dimensional systems [16] can also guide the investigation of such transitions in the physically realistic case of three dimensions. The behaviour of two layers of immiscible liquids sandwiched between a solid substrate and a gas (fig. 2) is governed by a van der Waals interface excess energy that depends on the thicknesses of both layers. Specifically, it contains three contributions $\Phi_{\mathrm{two}} = \Phi_{12g} + \Phi_{21s} + \Phi_{g21s}$ corresponding to the interactions of layer 1 with the gas across layer 2, of layer 2 with the substrate across layer 1 and of the gas with the substrate across layers 1 and 2, respectively. A flat two-layer film is linearly unstable if $(\partial^2_{h_1h_1}\Phi_{\mathrm{two}})(\partial^2_{h_2h_2}\Phi_{\mathrm{two}}) - (\partial^2_{h_1h_2}\Phi_{\mathrm{two}})^2 < 0$ or $\partial^2_{h_1h_1}\Phi_{\mathrm{two}} < 0$ [17]. This corresponds to an energy surface $\Phi_{\mathrm{two}}(h_1, h_2)$ that is concave or has a saddle point at the given thicknesses h_1 and h_2.

In the course of the time evolution the morphology of a two-layer film may change in various ways and at different stages of the evolution. One can distinguish the morphologies at the linear and the nonlinear stages of the short-time evolution and the one resulting in the long-time coarsening. Because of the relaxational nature of the thin-film time evolution the basic behaviour can be predicted from an analysis of the underlying energy functional in combination with a linear analysis of the time evolution. It is well known that the time evolution of both, one-layer [18] and two-layer [17], isothermal films can be modelled by a gradient dynamics for the energy functional F, given for a two-layer film by

$$F = \int \left[\sigma_{12}\frac{(\nabla h_1)^2}{2} + \sigma_2\frac{(\nabla h_2)^2}{2} + \Phi_{\mathrm{two}}\right] \mathrm{d}x\mathrm{d}y, \tag{1}$$

where σ_{12}, σ_2 are the interface tensions of the liquid-liquid and the liquid-gas interface, re-

spectively. The evolution equations for the film thicknesses h_1 and h_2 write [17,19,20]

$$\begin{aligned} \partial_t h_1 &= \nabla \left[Q_{11} \nabla \frac{\delta F}{\delta h_1} + Q_{12} \nabla \frac{\delta F}{\delta h_2} \right], \\ \partial_t h_2 &= \nabla \left[Q_{21} \nabla \frac{\delta F}{\delta h_1} + Q_{22} \nabla \frac{\delta F}{\delta h_2} \right], \end{aligned} \tag{2}$$

with the mobilities

$$\boldsymbol{Q} = \frac{1}{\mu_1} \begin{pmatrix} \frac{h_1^3}{3} & \frac{h_1^2}{2}(h_2 - \frac{h_1}{3}) \\ \frac{h_1^2}{2}(h_2 - \frac{h_1}{3}) & \frac{(h_2-h_1)^3}{3}(\frac{\mu_1}{\mu_2} - 1) + \frac{h_2^3}{3} \end{pmatrix}, \tag{3}$$

where μ_1 and μ_2 are the viscosities of liquid 1 and liquid 2, respectively.

Due to dissipation by viscous friction F decreases monotonically in time. Possible steady states make F extremal. Starting from the unstable flat film, a thickness profile approaches during its time evolution a number of steady states with consecutively decreasing energy. For one-layer films, typically, lower-energy steady states have a larger period, *i.e.* the surface patterns coarsen in time. In ref. [16] it was shown that this is not necessarily the case for two-layer systems. Using the two-dimensional case continuation techniques [21] were employed to study the minima of F. However, in the three-dimensional case the minima are not as easily accessible and we follow the time evolution by numerical integration of eqs. (2).

Following ref. [16], we specify Φ_{two} by combining destabilizing long-range van der Waals and stabilizing short-range polar interactions and nondimensionalize, resulting in the functional

$$\begin{aligned} F = \int \Big[&\frac{1}{2}(\nabla h_1)^2 + \frac{\sigma}{2}(\nabla h_2)^2 - \frac{\bar{A}_{12g}}{6(h_2 - h_1)^2} - \frac{\bar{A}_{21s}}{6h_1^2} - \frac{\bar{A}_{g21s}}{6h_2^2} + \\ &+ \bar{S}_1 \exp\left[-h_1\right] + \bar{S}_2 \exp\left[h_1 - h_2\right] \Big] \, \mathrm{d}x \, \mathrm{d}y. \end{aligned} \tag{4}$$

The nondimensional Hamaker constants are $\bar{A}_{ijkl} = \left[(d_2 - d_1)/l\right]^2 A_{ijkl}/|A_{12g}|$, and the short-range spreading coefficients are $\bar{S}_i = 2\pi \left[(d_2 - d_1)\right]^2 S_i \exp\left[d_0/l\right]/|A_{12g}|$. The scales for the lateral coordinates, time and energy are $l(d_2 - d_1)\sqrt{2\pi\sigma_1/|A_{12g}|}$, $(2\pi)^2\sigma_1\mu_1 l(d_2 - d_1)^4/A_{12g}^2$ and $|A_{12g}|/2\pi(d_2 - d_1)^2$, respectively.

The ratios of the mean layer thicknesses, surface tensions and viscosities are denoted, respectively, by $d = d_2/d_1$, $\sigma = \sigma_2/\sigma_1$ and $\mu = \mu_2/\mu_1$. The correlation length of the polar liquids l and the Born repulsion length d_0 are 1 to 10 nm and 0.158 nm, respectively [11]. For the present calculations we choose $d_i \gg l$, *i.e.* the short-range interactions do not influence the linear behaviour. Further on, we denote the scaled mean and local thicknesses by d_i and h_i, respectively. The nondimensional mobilities are given by eq. (3) dropping the prefactor $1/\mu_1$.

A linear stability analysis of a flat film using eqs. (2) shows two different unstable modes characterized by interface deflections that are in anti-phase (varicose) and in phase (zigzag), respectively. The global type of a profile can be quantified by the integral deflection measure

$$\phi_{\mathrm{int}} = \frac{1}{L} \int \frac{(h_1 - d_1)(h_2 - d_2)}{\left[(h_1 - d_1)^2 + (h_2 - d_2)^2\right]} \, \mathrm{d}x \, \mathrm{d}y. \tag{5}$$

This measure is valid for all stages of the evolution and is negative (positive) for varicose (zigzag) type profiles. A mode type change corresponds also to a transition of the three-dimensional surface morphology.

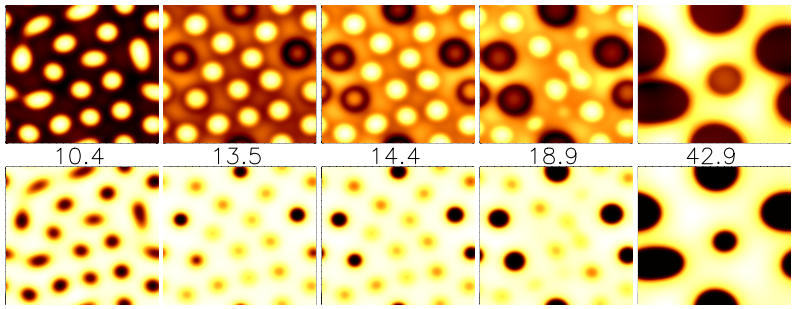

Fig. 3 – Time evolution of a Si/PMMA/PS/air system with mean thicknesses $d_1 = 20$, $d_2 = 30$. The upper (lower) row shows the top view of the liquid-gas (liquid-liquid) interface at indicated dimensionaless times t/τ. Dark (bright) regions correspond to lower (higher) values of the film thickness. The domain size is $5\lambda \times 5\lambda$.

In the following we demonstrate different transitions for a Si/PMMA/PS/air system fixing $A_{12g} = 1.49 \times 10^{-20}$ Nm, $A_{21s} = 3.8 \times 10^{-20}$ Nm, $A_{g21s} = -23.02 \times 10^{-20}$ Nm, $\bar{S}_1 = \bar{S}_2 = 1$, $\sigma = \mu = 1$. To estimate the characteristic growth time τ and wavelength λ of the instability we use $l \approx 1$ nm [11], $\sigma_1 \approx 2 \times 10^{-3}$ N/m [14] and $\mu_1 \approx 10^3$ kg/ms [22]. We numerically integrate eqs. (2) using flat films with small-amplitude random perturbations as initial conditions. The equations are solved with a semi-implicit pseudo spectral and a fully explicit integration scheme with 128×128 mesh points. The semi-implicit code is used in the linear stage of the evolution until the random perturbation has relaxed to a smooth surface showing the fastest growing wavelength in Fourier space. After that the fully explicit code is applied.

Transition via branch switching. We chose $d_1 = 20$, $d_2 = 30$ and obtain time sequences of interface profiles as shown in fig. 3. Typical scales are estimated to be $\tau \approx 3$ min and $\lambda \approx 0.6\,\mu$m. The evolution starts with a clear varicose mode (see fig. 4) corresponding to drops (holes) at the liquid-gas (liquid-liquid) interface (fig. 3, $t = 10.4$). Then a transition sets in between $t = 10.4$ and $t = 13.5$ turning droplets into ring-like ditches, *i.e.* holes with

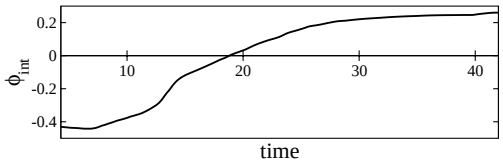

Fig. 4

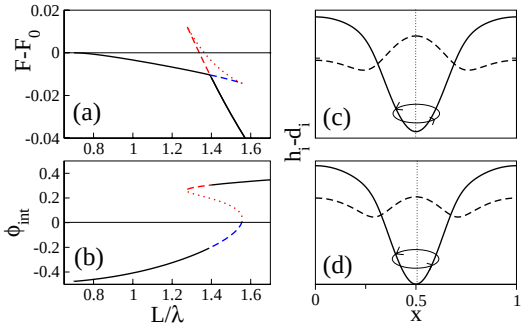

Fig. 5

Fig. 4 – Global deflection measure $\phi_{\rm int}$ (eq. (5)) *vs.* time t/τ for $d_1 = 20$, $d_2 = 30$.

Fig. 5 – (a) Relative energy and (b) global deflection measure of two-dimensional stationary solutions as functions of the period L/λ at $d_1 = 20$, $d_2 = 30$. (c) Low-energy stationary solution with $L/\lambda = 1.39$ and (d) high-energy stationary solution with $L/\lambda = 1.55$. In (c) and (d) solid (dashed) lines show the film thickness profiles at the liquid-liquid (liquid-gas) interfaces, respectively. The domain size is scaled to unity.

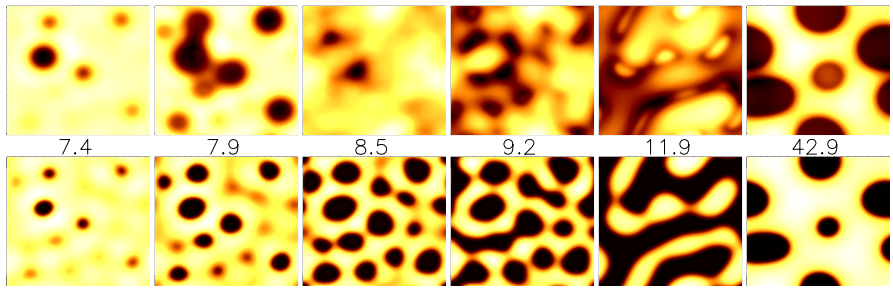

Fig. 6 – Time series analogous to fig. 3 but with mean thicknesses $d_1 = 15$ and $d_2 = 40$. The domain size is $5\lambda \times 5\lambda$.

a central elevation. The morphological transition does nearly not change the typical length scale, because it is not a consequence of coarsening but rather of switching between two stable solution branches. This is also indicated by the drastic increase in amplitude accompanying the transition. The height of the elevation then decreases gradually until at about $t = 18.8$ the rings have transformed into plain holes. In parallel the global deflection measure changes from varicose to zigzag (fig. 4). Later on coarsening takes over mainly through the merging of neighboring holes ($t > 20$).

It is possible to understand the transition *drops-rings-holes* by studying two-dimensional steady solutions of eqs. (2) using continuation techniques [21]. Starting from the analytically known small-amplitude solution with a period corresponding to the critical wavelength L_c obtained from the linear stability analysis, one obtains multivalued solution branches as characterized in fig. 5 by their relative energy $(F - F_0)$ and the global deflection measure $\phi_{\rm int}$ in dependence of period L (in units of λ).

The solid and the dashed lines in fig. 5(a, b) correspond both to linearly stable solutions (at the respective L, they are unstable to slow coarsening modes). However, only the solid lines correspond to global minima, whereas the dashed lines refer to local minima. For periods $L > 1.39$, the energetically preferable solution is of zigzag type whereas the local minimum is of varicose type (fig. 5(b)). This explains the persistence of the length scale during the transition because the morphology change occurs via branch switching, *i.e.* the evolution "jumps" from one stable solution branch to another one of lower energy.

The global deflection measure $\phi_{\rm int}$ of the high-energy solutions (dashed line) is negative at $L = 1.39$ and almost equals zero at $L = 1.55$. Figures 5(c) and (d) show stationary solutions from the stable low-energy branch at $L = 1.39$ and from the stable high-energy branch at $L = 1.55$, respectively. One can see that the liquid-gas interface (dashed line) has

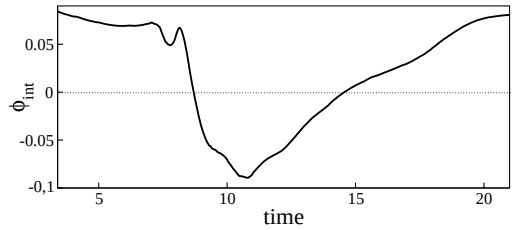

Fig. 7 – Global deflection measure $\phi_{\rm int}$ *vs.* time t/τ for the evolution shown in fig. 6.

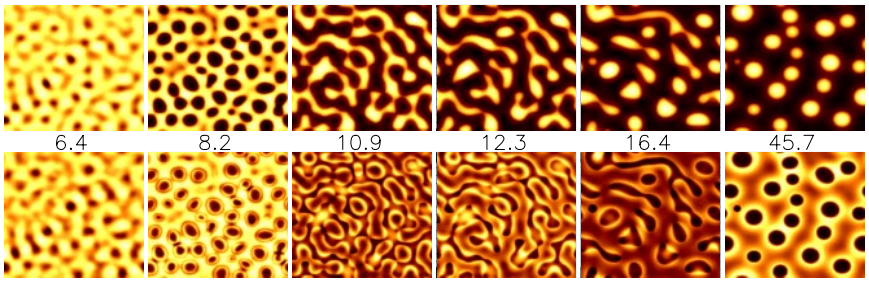

Fig. 8 – Time series of the evolution of the SiO/PMMA/PS/air system with $d_1 = 20$ and $d_2 = 40$. The domain size is $7\lambda \times 7\lambda$ (256×256 mesh points).

two depressions beside the drop-like elevation in the center. Imagine to rotate the profiles around a vertical axis at $x = 0.5$. The resulting rotationally symmetric surface pattern strongly resembles the rings found in the simulation (fig. 3).

Transition via coarsening. Beside the described drop-ring-hole transition, one can also find a hole-drop transition just by changing the mean-film thicknesses. We chose $d_1 = 15$, $d_2 = 40$ and obtain time sequences of interface profiles as shown in fig. 6. Typical scales are estimated to be $\tau \approx 20\,\text{min}$ and $\lambda \approx 1.0\,\mu\text{m}$. The evolution starts with a zigzag mode (see fig. 7) corresponding to holes at both interfaces. The zigzag mode dominates only in the linear stage of the evolution. With increasing amplitudes the system switches in a complicated process to varicose-type profiles corresponding also to the steady state of corresponding period for a two-dimensional system. First, the pattern seems to coarsen because neighboring holes merge (at the liquid-gas interface, $t = 7.9$). However, they split again into holes shifted with respect to the original ones, thereby changing the profile to varicose type ($t = 8.5$). The morphology at the liquid-liquid interface remains unchanged. Later on, coarsening truly sets in accompanied by a transition involving both interfaces. Passing through intermediate labyrinths ($t = 11.9$) drops prevail at both interfaces showing clear zigzag type ($t = 22.4$). In contrast to the above transition via branch switching, this involved morphology transition is intrinsically related to coarsening.

SiO/PMMA/PS/air system. Finally, we study the evolution of another experimentally investigated system [14], SiO/PMMA/PS/air. We use $A_{12g} = 1.49 \times 10^{-20}\,\text{Nm}$, $A_{21s} = -0.02 \times 10^{-20}\,\text{Nm}$, $A_{g21s} = 0.15 \times 10^{-20}\,\text{Nm}$, $\bar{S}_1 = \bar{S}_2 = 1$, $d_1 = 20$ and $d_2 = 40$, resulting in $\tau \approx 100\,\text{h}$ and $\lambda \approx 20\,\mu\text{m}$.

Figure 8 shows the time series of the evolution. At the early stage rings appear at the liquid-liquid and holes at the liquid-gas interface ($t = 8.2$). These patterns are of zigzag type (see fig. 9) and have a characteristic size corresponding to the fastest growing linear mode. The patterns are not steady because, as a two-dimensional analysis shows, there exists only a steady

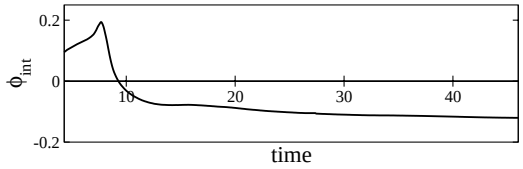

Fig. 9 – Global deflection measure ϕ_{int} *vs.* time t/τ for the SiO/PMMA/PS/air system at $d_1 = 20$ and $d_2 = 40$.

varicose-type profile of this size (not shown). Later on, the holes at the liquid-gas interface turn into drops ($t = 16.4$) via labyrinths ($t = 10.9$), whereas the rings at the liquid-liquid interface transform via labyrinths into circular holes, surrounded by an elevated region ($t = 45.7$).

As for the one-layer system also for two layers the equilibrium film thicknesses found at long times may be obtained by a Maxwell construction. However, in contrast to the case of one layer, here two Lagrange multipliers (corresponding to material conservation for the two layers) have to be adjusted to tilt the energy landscape $f(h_1, h_2)$ correspondingly (similar to finding the equilibrium concentrations for a decomposing ternary mixture). This may lead to a multiplicity of solutions even in the long-time limit as observed here for a restricted range of structure sizes.

To conclude, we have investigated the structuring process of two-layer films driven by destabilizing van der Waals interactions in three dimensions. We have described different types of morphological transitions occurring in the course of the short- and long-time evolution. We have illustrated that the here defined global deflection measure faithfully indicates visible changes of the surface morphology. For instance, for the Si/PMMA/PS/air system the branch switching transition from varicose to zigzag type corresponds to the transition from drops to holes at the liquid-gas interface. For the SiO/PMMA/PS/air system, however, the holes at the liquid-gas interface turn into drops corresponding to a change of mode type from zigzag to varicose. We are optimistic that the presented results make it worthwhile to extend the first experimental investigations [12–15] of the structuring of two-layer films and to focus on the morphological transitions involved.

REFERENCES

[1] Reiter G., *Phys. Rev. Lett.*, **68** (1992) 75.
[2] Israelachvili J. N., *Intermolecular and Surface Forces* (Academic Press, London) 1992.
[3] Oron A., Davis S. H. and Bankoff S. G., *Rev. Mod. Phys.*, **69** (1997) 931.
[4] Thiele U., *Eur. Phys. J. E*, **12** (2003) 409.
[5] Bestehorn M. and Neuffer K., *Phys. Rev. Lett.*, **87** (2001) 046101.
[6] Thiele U., Velarde M. G. and Neuffer K., *Phys. Rev. Lett.*, **87** (2001) 016104.
[7] Bestehorn M., Pototsky A. and Thiele U., *Eur. Phys. J. B*, **33** (2003) 457.
[8] Sharma A. and Khanna R., *Phys. Rev. Lett.*, **81** (1998) 3463.
[9] Pismen L. M. and Pomeau Y., *Phys. Rev. E*, **62** (2000) 2480.
[10] Thiele U., Neuffer K., Pomeau Y. and Velarde M. G., *Colloid Surf. A*, **206** (2002) 135.
[11] Sharma A., *Langmuir*, **9** (1993) 861.
[12] Faldi A., Composto R. J. and Winey K. I., *Langmuir*, **11** (1995) 4855.
[13] David M. O., Reiter G., Sitthai T. and Schultz J., *Langmuir*, **14** (1998) 5667.
[14] Sferrazza M., Heppenstall-Butler M., Cubitt R., Bucknall D., Webster J. and Jones R. A. L., *Phys. Rev. Lett.*, **81** (1998) 5173.
[15] Wunnicke O., Müller-Buschbaum P., Wolkenhauer M., Lorenz-Haas C., Cubitt R., Leiner V. and Stamm M., *Langmuir*, **19** (2003) 8511.
[16] Pototsky A., Bestehorn M., Merkt D. and Thiele U., *J. Chem. Phys.*, **122** (2005) 224711.
[17] Pototsky A., Bestehorn M., Merkt D. and Thiele U., *Phys. Rev. E*, **70** (2004) 025201(R).
[18] Mitlin V. S., *J. Colloid Interface Sci.*, **156** (1993) 491.
[19] Fisher L. S. and Golovin A. A., *J. Colloid Interface Sci.*, **291** (2005) 515.
[20] Bandyopadhyay D., Gulabani R. and Sharma A., *Ind. Eng. Chem. Res.*, **44** (2005) 1259.
[21] Doedel E. J., Champneys A. R., Fairgrieve T. F., Kuznetsov Y. A., Sandstede B. and Wang X. J., *AUTO97: Continuation and Bifurcation Software for Ordinary Differential Equations* (Concordia University, Montreal) 1997.
[22] Tchomakov K. P., Favis B. D., Huneault M. A., Champagne M. F. and Tofan F., *Polym. Eng. Sci.*, **44** (2004) 749.